Machine Learning of Atomic Forces from Quantum Mechanics: a Model Based on Pairwise Interatomic Forces

I. Ramzan,[a] L. Kong,[a] R. A. Bryce[a,*] and N. A. Burton[b,*]

[a] Division of Pharmacy and Optometry, School of Health Sciences, University of Manchester, Oxford Road, Manchester M13 9PL, UK. and [b] Department of Chemistry, University of Manchester, Oxford Road, Manchester M13 9PL, UK.

* Correspondence should be addressed to:

Richard A Bryce (richard.bryce@manchester.ac.uk), Division of Pharmacy and Optometry, School of Health Sciences, Faculty of Biology, Medicine and Health, University of Manchester, Oxford Road, Manchester M13 9PL, UK. Tel (0)161 275 8345. ORCID 0000-0002-8145-2345

or Neil A Burton (neil.burton@manchester.ac.uk) Department of Chemistry, University of Manchester, Oxford Road, Manchester M13 9PL, UK. ORCID 0000-0001-5773-3844

Keywords: interatomic forces, quantum mechanics, machine learning, artificial neural network, pairwise force decomposition, molecular dynamics simulation

Abstract

We present a new chemically intuitive approach, pairF-Net, to directly predict the atomic forces in a molecule to quantum chemistry accuracy using machine learning techniques. A residual artificial neural network has been designed and trained with features and targets based on pairwise interatomic forces, to determine the Cartesian atomic forces suitable for use in molecular mechanics and dynamics calculations. The scheme implicitly maintains rotational and translational invariance and predicts Cartesian forces as a linear combination of a set of force components in an interatomic basis. We show that the method can predict the reconstructed Cartesian atomic forces for a set of small organic molecules to less than 2 kcal mol^{-1} $Å^{-1}$ from the reference force values obtained via density functional theory. The pairF-Net scheme utilises a simple and chemically intuitive route to furnish atomic forces at a quantum mechanical level but at a fraction of the cost, providing a step towards the efficient calculation of accurate thermodynamic properties.

1. Introduction

The mechanics, dynamics and thermodynamics of molecular systems is governed by the forces acting between atoms. The quest to obtain accurately predicted macroscopic properties from materials to biomolecules has advanced significantly in recent years, with developments in computational hardware and algorithms permitting longer time scale molecular dynamics (MD) simulations.[1] These simulations are better able to probe the equilibrium behaviour of long time scale events such as a protein's folding[2] and binding to ligands,[3] as well as the conformational manifold of small molecules in solution.[4-5] However, the forces underpinning these long simulations are typically computed via empirically derived potential functions. The ability to more robustly compare experimental data, such as from NMR measurements, with converged simulated properties has exposed shortcomings in such force fields[6] and points to the need for the use of higher accuracy forces in MD simulations. This is particularly true for small organic molecules, where the large diversity of chemistry present across this chemical space[7] is coupled to a lack of maturity in the force field models of their behaviour.[8]

The empirical function of a force field approximates the quantum mechanical (QM) interactions in a molecule. These forces contain electrostatic and van der Waals two-body effects but also subtle factors arising from electronic polarization and charge transfer that are less readily captured by force fields. Until recently, the ability to incorporate quantum chemical forces into molecular simulations has been limited to very short timescales, due to the aggregate computational expense of the QM force evaluation required at each time step. However, recent efforts have deployed machine learning (ML) approaches to bridge this gap,[9] seeking to furnish energies[10-13] and more recently forces[14-19] of QM accuracy at a fraction of the computational cost. Using large datasets of molecular geometry, energy and forces, ML methods such as kernel-based methods and artificial neural nets (ANNs) have been trained to provide

interpolated energy and force predictions. Commonly used benchmark data sets of QM data for this purpose include the QM7,[20] QM9[21] and MD17 data sets,[17] as well as the recently developed COMP6 set.[22]

Within this broad philosophy, a range of approaches have been adopted: for example, in the SchNet method,[18] a convolutional neural network is trained using QM energies and forces. The gradient-domain machine learning (GDML) method[17] is a kernel-based method that learns forces directly. Similarly, the AGNI machine learned force field[16] uses kernel ridge regression as the means to directly learn QM forces. In the ANAKIN-ME (ANI) approach,[10, 15] the QM energy of a diverse range of molecules was learned via an ANN and then a force on the atoms was subsequently obtained by taking the derivative of the trained network. The ANI approach uses a modified version of single atom symmetry function as descriptors of the atomic environment.[23] Determining these functions for diverse heteroatomic chemical systems is a challenging task. For direct learning of forces, a vector property, radial shells engendered by this characterisation of the atomic environment would not appear well suited.

As an alternative to symmetry functions, Zhang et al.[19] developed a molecular representation in terms of a local reference frame based on pairwise distances R_{ij} between atoms and a local environment for each atom. Specifically, within a given cutoff radius around an atom i, radial and angular information is gathered, forming the set, $D_{ij}= \{1/R_{ij}, x_{ij}/R_{ij}^2, y_{ij}/R_{ij}^2, z_{ij}/R_{ij}^2\}$. Based on these input features, a neural network with five hidden layers was then trained to reproduce the total potential energy of the configuration (the sum of atomic energies, E_i), using per atom energies, Cartesian forces and virial in the loss function. The method, which they called deep potential molecular dynamics (DPMD), was able to reproduce ab initio QM forces acting on water and ice at different temperatures and pressures to around 1 kcal mol^{-1} Å^{-1} of the PBE0 +

vdW-TS density functional value;[24-25] a similarly good performance was obtained for reproducing the PBE + vdW-TS forces within small organic molecules.

In this work, we develop a neural network approach based on pairwise forces, which we denote the pairF-Net method. For this, we explicitly employ an interatomic internal representation of the molecular structure for the evaluation of translationally and rotationally invariant atomic Cartesian forces. Recognising that the atomic forces determined using a quantum mechanical potential are a combination of nuclear repulsion and electronic terms, we exploit this partition to use an appropriately trained residual feedforward neural network to predict the total or electronic contribution to the atomic forces in a molecule.

In the spirit of the Coulomb matrix approach utilised by other workers as input to their energy prediction machine learning schemes,[9] we explicitly use the negative derivatives of nuclear repulsion energies, the nuclear repulsion forces (NRFs), as input to our force-predicting network. Thus, the NRFs play a dual role, principally as features which usefully and completely encode the molecular structure; and secondly, to focus learning on the chemically important electronic contribution to the forces. As we shall show, as with molecular energies, because the total forces are the difference in nuclear and electronic terms, both of which have large magnitudes, it will be important that the predicted total resultant forces have a small variance and few outliers for accurate prediction of forces, rather than just a low mean error.

An attractive feature of the pairF-Net scheme is that both the NRFs and the predicted total forces are expressed in an interatomic basis, $\{q_{AB}^{\mathrm{NR}}\}$ and $\{q_{AB}^{\mathrm{ANN}}\}$ respectively, and are therefore invariant to translation and rotation of the molecule. The use of such an internal coordinate system allows us to draw upon chemically useful concepts of interatomic forces to aid our

understanding of the nuances of the scheme, and provides a foundation for future approximations and transferability. The final step in our scheme is a simple linear transformation of the predicted interatomic forces $\{\mathbf{Q}_{AB}\}$, back to the Cartesian basis of the molecular structure to give the Cartesian atomic forces, $\{\mathbf{F}_A\}$, required for geometry optimisation or molecular dynamics simulations.

In order to train the ANN, it is therefore necessary to decompose the total quantum mechanical Cartesian atomic forces to the interatomic basis. We linearly transform these Cartesian exact forces $\{\mathbf{F}_A^{\mathrm{QM}}\}$ into the interatomic basis by performing a pairwise decomposition using an approach previously used for vibrational analysis[26] and in redundant coordinate optimisation schemes.[27] An analogous scheme was used to generate internal forces to understand the mechanical stress in molecules.[28-29] The resulting interatomic forces, $\{\mathbf{Q}_{AB}^{\mathrm{QM}}\}$, form a complete set such that not only two-body but three-body and higher terms are also captured exactly.

Overall, we may view the use of the ANN in the pairF-Net approach as either a functional of the NRFs, $\mathbf{F}[\mathbf{q}^{\mathrm{NR}}(\mathbf{R})]$, or alternatively, as a predictor of corrections to the NRFs, to estimate accurate QM atomic forces. Although other machine learning approaches can be applied, here we have chosen to generate the predictions of $\{q_{AB}^{\mathrm{ANN}}\}$ via a sequentially constructed residual artificial neural network. This approach is able to fit unknown non-linear functions of great complexity, and also allows industry standard software such as TensorFlow[30]and Keras[31] to be utilised.

In the following sections, we describe in more detail the pairF-Net scheme and its implementation, including design of network architectures; we consider the ability of the decomposition of Cartesian atomic forces to produce chemically reasonable pairwise forces;

and we evaluate the accuracy of pairF-Net in generating atomic forces for small molecule systems.

2. The PairF Scheme

2.1 Definition of Atomic Forces in a Cartesian framework

Firstly, we introduce the definitions for Cartesian atomic forces, as required for molecular mechanics and dynamics calculations. For an isolated quantum mechanical molecular system, the total molecular potential energy, E^{QM}, can be obtained from the Schrödinger equation within the Born-Oppenheimer approximation as a sum of nuclear and electronic Hamiltonians,

$$\widehat{H}(\mathbf{r},\mathbf{R}) = \widehat{H}^{\mathrm{nuc}}(\mathbf{R}) + \widehat{H}^{\mathrm{elec}}(\mathbf{r},\mathbf{R}) \tag{1}$$

and hence the potential energy of the system will be

$$E^{\mathrm{QM}}(\mathbf{r},\mathbf{R}) = E^{\mathrm{NR}}(\mathbf{R}) + E^{\mathrm{elec}}(\mathbf{r},\mathbf{R}) \tag{2}$$

where **r** and **R** are the electron and nuclear coordinates, respectively. The nuclear repulsion energy (NRE) is given in atomic units as

$$E^{\mathrm{NR}} = \sum_{A}^{N}\sum_{B<A}^{N}\frac{Z_A Z_B}{R_{AB}} \tag{3}$$

where Z_A and Z_B are the charges of nuclei *A* and *B*, respectively. $R_{AB} = |\mathbf{R}_B - \mathbf{R}_A|$ with $\mathbf{R}_A$ and $\mathbf{R}_B$ the position Cartesian coordinates of atom *A* and *B* respectively. The second term, E^{elec}, is the electronic energy. The Cartesian forces acting on atom *A*, $\mathbf{F}_A^{\mathrm{QM}}$, are then given by

$$\mathbf{F}_A^{\mathrm{QM}} = -\boldsymbol{\nabla}_A E^{\mathrm{QM}} = -\boldsymbol{\nabla}_A E^{\mathrm{NR}} - \boldsymbol{\nabla}_A E^{\mathrm{elec}} = \mathbf{F}_A^{\mathrm{NR}} + \mathbf{F}_A^{\mathrm{elec}} \quad (4)$$

where $\boldsymbol{\nabla}_A = \left(\frac{\partial}{\partial R_{A,x}}, \frac{\partial}{\partial R_{A,y}}, \frac{\partial}{\partial R_{A,z}}\right)^T$ and $\partial R_{A,k}$ are the Cartesian displacements of atom *A*.

This total atomic force is a vector in the Cartesian basis given by

$$\mathbf{F}_A^{\mathrm{QM}} = f_A \mathbf{e}_A \quad (5)$$

where the magnitude and direction of the force are f_A and $\mathbf{e}_A$ respectively, with $\|\mathbf{e}_A\| = 1$. For an isolated system of *N* atoms, the Cartesian forces $\mathbf{F}^{\mathrm{QM}}$ will comprise all 3*N* Cartesian force components, $\{f_A e_{(A,k)}\}$, arranged here as a vector rather than a $3 \times N$ matrix. The individual elements of this vector are

$$F_{(A,k)}^{QM} = f_A e_{(A,k)} = -\left(\frac{\partial E^{QM}}{\partial R_{(A,k)}}\right)_{\mathbf{R}_B} \quad (6)$$

where E^{QM} is the total potential energy; and $R_{(A,k)}$ are the Cartesian components of $\mathbf{R}_A$, the position vector of atom *A*, where $k = \{x, y, z\}$, with respect to the Cartesian origin.

2.2 Interatomic Force Components

To determine the interatomic force components according to the pairF scheme, we require the expression of Cartesian atomic forces within an internal coordinate frame. Let us consider the resolution of an atomic force acting on atom *A*, $\mathbf{F}_A$, in a Cartesian coordinate basis, into a set

of interatomic force components, $\{\mathbf{Q}_{BA}\}$, each acting on atom *A* along the vector $\overrightarrow{BA}$ from atom *B*,

$$\mathbf{F}_A = \sum_{B \neq A}^{N-1} \mathbf{Q}_{AB} \quad . \tag{7}$$

Equation 7 simply states that a set of force component vectors $\mathbf{Q}_{AB}$ acting on each atom A can be linearly combined to give a resultant force vector on each atom; this is illustrated for a model three atom system in Figure 1. The sum here is over all unique atom pairs and will be referred to as the interatomic basis. To maintain generality, we use the term intermolecular force components rather than intermolecular forces.

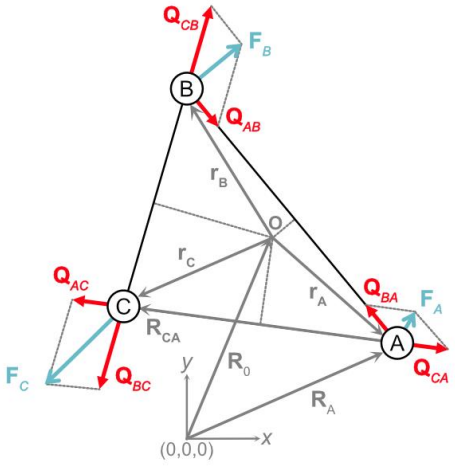

Figure 1 Schematic of the internal resolution of the forces in a three-atom system, where A, B and C are atoms, O is the centre of mass, **F** are the forces in a Cartesian framework, **Q** are the interatomic force component vectors, and **R** and **r** are position vectors.

The force component vectors in the interatomic basis are defined as

$$\mathbf{Q}_{AB} = q_{AB}\mathbf{e}_{AB} \quad \text{or} \quad Q_{(AB,k)} = q_{AB}e_{(AB,k)} \tag{8}$$

where $\mathbf{e}_{AB} = \frac{(\mathbf{R}_B - \mathbf{R}_A)}{\|\mathbf{R}_B - \mathbf{R}_A\|} = \frac{(\mathbf{R}_B - \mathbf{R}_A)}{\|\mathbf{R}_{AB}\|} = \frac{(\mathbf{R}_B - \mathbf{R}_A)}{R_{AB}} = -\mathbf{e}_{BA}$ where $\|\mathbf{e}_{BA}\| = 1$, and $\mathbf{q}$ is the vector of the $\{q_{AB}\}$ magnitudes, hereafter referred to as the *interatomic* or *pair force components*. For a two-body potential, the interatomic force for atom *B* acting on atom *A* would be given by q_{AB}, where $\mathbf{Q}_{AB} = q_{AB}\mathbf{e}_{AB} = -q_{AB}\mathbf{e}_{BA}$, and the unit vectors $\mathbf{e}_{AB} = \overrightarrow{BA}/\left|\overrightarrow{BA}\right| = -\mathbf{e}_{AB}$. This follows the normal convention that a positive value of q is indicative of repulsion, and negative of attraction.

Although there are many other possible internal representations of a molecular structure, for example using specific combinations of bond lengths, angles and dihedrals, the full set of all interatomic distances between all atom pairs $\{R_{AB}\}$ used in this work serves to completely define any possible structure. Although the set may be reduced towards a minimal set of 3*N*–6 terms required to define the structure of a non-linear molecule, dependence on specific conformers or isomers of the molecule, and problems with linear dependence of a reduced set, are avoided when using the full expansion. Nevertheless, the pairF-Net approach explored in this work can be readily adapted to a reduced basis, which may be prudent as the size of the system increases.

In the absence of external forces, the Cartesian atomic forces will not be linearly independent since they should implicitly include the three translational and three rotational constraints such that

$$\boldsymbol{\varepsilon}_{\text{translation}} = \sum_{A=1}^{N} \mathbf{F}_A^{\text{QM}} = \mathbf{0} \tag{9}$$

and

$$\boldsymbol{\varepsilon}_{\text{rotation}} = \sum_{A=1}^{N}\left(\mathbf{r}_A \times \mathbf{F}_A^{\text{QM}}\right) = \mathbf{0} \tag{10}$$

respectively, where $\mathbf{r}_A = \mathbf{R}_A - \mathbf{R}_0$ and the rotational centre is given by

$$\mathbf{R}_0 = \frac{1}{N}\sum_{A=1}^{N}\mathbf{R}_A \quad . \tag{11}$$

Taking these constraints into account yields the familiar result that there are $3N - 6$ linearly independent internal forces acting within the system. Equation 7 can now be rewritten in the interatomic basis with the following linear transformation,

$$\mathbf{F}_A \; = \mathbf{T}_A\,\mathbf{q} = \sum_{B\neq A} q_{AB}\cdot\mathbf{e}_{AB} \tag{12}$$

which can be generalised for a non-linear *N*-atom system to

$$\mathbf{F} = \mathbf{T}\,\mathbf{q} \tag{13}$$

where the transformation coefficients are given by

$$T^{AB}_{(A,k)} = e_{(AB,k)} \text{ and } T^{AB}_{(B,k)} = -e_{(BA,k)} \quad . \tag{14}$$

Since the total number of unique interatomic forces between all pairs of atoms is $N(N-1)/2$, there will be twice as many, component force vectors Q_{AB}, namely $N^{\mathrm{Q}} = N(N-1)$. The dimension of $\mathbf{q}$, the total number of unique *component force magnitudes*, will therefore be $N^{\mathrm{q}} = N(N-1)/2$, i.e. $N^{Q}/2$, since each vector has an equal but opposite partner, $\mathbf{Q}_{AB} = -\mathbf{Q}_{BA}$. Importantly, as with two-body interactions, each interatomic force component has the

property of translational and rotational invariance. This will mean that these components may be predicted independently and, no matter their individual errors, their sums,

$$\boldsymbol{\varepsilon}_{\text{translation}} = \sum_A^N \sum_{B \neq A}^N \mathbf{Q}_{AB} = \mathbf{0} \tag{15}$$

and

$$\boldsymbol{\varepsilon}_{\text{rotation}} = \sum_A^N \sum_{B \neq A}^N (\mathbf{r}_A \times \mathbf{Q}_{AB}) = \mathbf{0} \tag{16}$$

and Cartesian forces obtained from these *via* Equation 13 will also be invariant, obeying Equations 9 and 10.

2.3 Implementation of the pairF-Net Model

In the Cartesian basis, the force on atom *A* arising from the nuclear repulsion term in the Hamiltonian (Equation 4) is given by,

$$\mathbf{F}_C^{\text{NR}} = -\boldsymbol{\nabla}_C E^{\text{NR}} = \sum_{A \neq C}^N \frac{Z_A Z_C}{(R_{AC})^2} \mathbf{e}_{AC} \quad . \tag{17}$$

If expressed in an interatomic basis, the magnitude of the nuclear repulsion force for the atom pair *A* and *B* is

$$q_{AB}^{\text{NR}} = -\frac{\partial E^{\text{NR}}}{\partial R_{AB}} = \frac{Z_A Z_B}{(R_{AB})^2} \quad . \tag{18}$$

We shall refer to q_{AB}^{NR} as a nuclear repulsion force or NRF, although more precisely, it should be denoted as the internuclear repulsion force. Thus the total magnitude of the force for atom pair *A* and *B* in the interatomic basis is

$$q_{AB}^{\mathrm{QM}} = q_{AB}^{\mathrm{NR}} + q_{AB}^{\mathrm{elec}} \tag{19}$$

or

$$\mathbf{q}^{\mathrm{QM}} = \mathbf{q}^{\mathrm{NR}} + \mathbf{q}^{\mathrm{elec}} \ . \tag{20}$$

We emphasise that in the pairF-Net scheme, the force components $\{q_{AB}^{\mathrm{QM}}\}$ or $\{q_{AB}^{\mathrm{elec}}\}$ used to train the ANN are not directly derived as derivatives of the potential, but instead are obtained by decomposing the Cartesian atomic forces into the interatomic basis as described in the next section. We shall refer to the forces in the interatomic basis which are used to train the ANN as $\{q_{AB}^{\mathrm{Ref}}\}$ or $\mathbf{q}^{\mathrm{Ref}}$.

The forces predicted by the ANN will be a functional of the input parameters used to encode the molecular structure. In this work, we have chosen the input features to the pairF-Net ANN to be the complete set of N^{q} NRFs, $\{q_{AB}^{\mathrm{NR}}\}$, rather than to decompose the Cartesian derivatives of the NRE. For expediency, in the residual network architecture which we have implemented, the NRFs are trivial to compute and it becomes convenient to fit the forces using one of the two following schemes.

In the first training scheme, which we label **D1**, the goal is to predict the total interatomic force components directly,

$$\mathbf{q} = \mathbf{q}^{\mathrm{ANN}}, \tag{21}$$

based upon fitting the ANN with $\mathbf{q}^{\mathrm{Ref}} = \mathbf{q}^{\mathrm{QM}}$.

In the second training scheme, **D2**, the aim is to predict the forces by recombining the force predictions of an electronic component with the NRFs to give the total interatomic forces,

$$\mathbf{q} = s^{\mathrm{NR}}\ \mathbf{q}^{\mathrm{NR}} + \mathbf{q}^{\mathrm{ANN}} \tag{22}$$

based upon fitting the ANN with $\mathbf{q}^{\mathrm{Ref}} = \mathbf{q}^{\mathrm{QM}} - s^{\mathrm{NR}}\ \mathbf{q}^{\mathrm{NR}}$. In the simplest case, where $s^{\mathrm{NR}} = 1$, the pairF-Net ANN is trained to predict solely the electronic component $\mathbf{q}^{\mathrm{Ref}} = \mathbf{q}^{\mathrm{elec}}$. Although this approach is fundamentally the same as Equation 13, we will subsequently show that since the force components are not exact potential derivatives, practical numerical issues will favour training using reference scheme **D1**.

In both scenarios, the loss function $\left\|\mathbf{q}^{\mathrm{Ref}} - \mathbf{q}^{\mathrm{ANN}}\right\|_2^2$ is minimised for the training set of structures and the recombination step to convert the forces to the Cartesian basis will be

$$\mathbf{F}^{\mathrm{ANN}} = \mathbf{T}\ \mathbf{q}^{\mathrm{ANN}}\ . \tag{23}$$

As noted in the previous section, each individual interatomic force component is invariant to translation or rotation of the molecular framework and the resulting atomic Cartesian forces will retain this property. This is an important feature of pairF-Net, since the invariance does not need to be explicitly included in the loss function, for example to ensure that $\mathbf{F}_A = -\boldsymbol{\nabla}_A E$, which is necessary for methods based on direct prediction of Cartesian forces.[17]

2.4 Computation of Interatomic Force Components

In order to train pairF-Net, it is necessary to transform each set of reference Cartesian atomic forces to an interatomic basis. Since both the Cartesian and full interatomic bases are over-representative of the system, this may be accomplished using the generalised inverse of Equation 13,

$$\mathbf{q} = \mathbf{T}^{+}\mathbf{F} + (\mathbf{I} - \mathbf{T}^{+}\mathbf{T})\,\mathbf{m} \quad . \tag{24}$$

Here $\mathbf{T}^{+} = (\mathbf{T}^{T}\mathbf{T})^{-1}\,\mathbf{T}^{T} = \mathbf{T}^{-}\mathbf{T}^{T}$ is recognisable as the Moore-Penrose pseudoinverse (i.e. the left inverse), where $\mathbf{T}^{-} = (\mathbf{T}^{T}\,\mathbf{T})^{-1}$ and $\mathbf{T}^{+}\mathbf{T} = \mathbf{I}$ (noting *T* as the matrix transpose). Although this equation has general solutions, for any vector **m**, a somewhat unique solution,

$$\mathbf{q}^{0} = \mathbf{T}^{+}\mathbf{F}\,, \tag{25}$$

can be obtained by this approach with $\mathbf{m} = \mathbf{0}$; this is the so-called solution with minimum Euclidian norm, such that $\|\mathbf{q}^{0}\|_2 \leq \|\mathbf{q}\|_2$. Although there are an infinity of other possible solutions ($\mathbf{m} \neq \mathbf{0}$), this constraint on the norm implies that within the set $\mathbf{q}^{0}$, each individual force component will have its minimum magnitude allowed, provided the set as a whole satisfies Equation 13. This feature of the minimum norm $\mathbf{q}^{0}$ solution, together with it being a continuous function of **R**, usefully correlates with our expectations of a unique force component between each specific pair of atoms which is applicable to the whole potential energy surface. However, we must stress that the force components **q** are not derivatives of the original molecular potential and we must be careful to respect that their relative magnitudes, and particularly their signs, may not always correspond to a physical interpretation of an electronic or total force.

In this work, the transformation coefficients are given by Equation 14. However, we note an alternative to obtaining alternative solutions from the full Moore-Penrose inverse with $\mathbf{m} \neq 0$, such that we may use a biased transformation *via* a scaled basis, $\gamma_{AB} \neq 1$, to obtain a different balance of forces between different atom pairs,

$$T_{(A,k)}^{AB(\text{bias})} = \gamma_{AB} e_{(AB,k)} \text{ and } T_{(B,k)}^{AB(\text{bias})} = -\gamma_{AB} e_{(BA,k)}. \quad (26)$$

The force components obtained using the biased basis transformation, $\mathbf{q}^{\text{bias}}$, can then be re-scaled to the original unbiased basis, $q_{AB} = \gamma_{AB} q_{AB}^{\text{bias}}$, in order to train the ANN and predict unknown forces using the unbiased transformation.

Since to train pairF-Net, it is necessary to decompose the reference Cartesian atomic forces to the internal interatomic basis,

$$\mathbf{q} = \mathbf{T}^{+}\,\mathbf{F}, \quad (27)$$

an advantage of this approach is that the transformation of the Cartesian forces to the internal basis will remove any residual translational or rotational invariance which might be present in the Cartesian basis. It is not unsual for the atomic forces from QM methods to have some residual rotational and translational force, such that $\boldsymbol{\varepsilon}_{\text{rotation}} \neq 0$ and $\boldsymbol{\varepsilon}_{\text{translation}} \neq 0$ in Equations 9 and 10 respectively. This can particularly be the case for smaller atom-centred basis sets, or when numerical integration is used in density functional theory. If the QM forces have numerical issues, then it would be important to ensure that any assessments of the quality of predicted forces are also assessed against comparable invariant forces.

To summarise, Cartesian forces obtained from QM calculation $\mathbf{F}_A^{\mathrm{QM}}$ are decomposed into interatomic force components, $\mathbf{q}^{\mathrm{Ref}}$ (Figure 2); the latter then provide target values for training of the ANN, along with input features provided by the nuclear repulsion forces, $\mathbf{q}^{\mathrm{NR}}$. The ANN is trained to predict $\mathbf{q}^{\mathrm{Ref}}$, corresponding to either the total forces, $\mathbf{q}^{\mathrm{QM}}$ (**D1**), or the electronic component of these, $\mathbf{q}^{\mathrm{elec}}$ (**D2**); these interatomic forces are then recombined to provide total Cartesian forces acting on atoms.

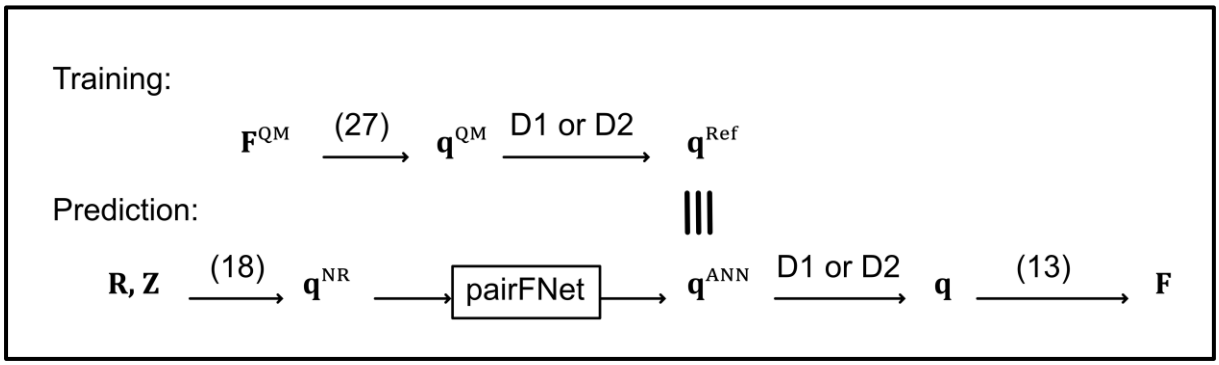

Figure 2 Summary of workflow to train pairF-Net and predict atomic forces **F** via training scheme **D1** or **D2**.

3. Computational Details

3.1 Network Design

To learn and predict the pairwise forces $\mathbf{q}^{\mathrm{QM}}$ or $\mathbf{q}^{\mathrm{elec}}$, we construct a series of neural networks with a modular feed-forward structure (Figure 3a). Each network comprises an input block (IB, Figure 3a), one or more hidden network blocks (NB) and then an output block. Each block is fully connected to the next. The input block of N^{q} neurons receives a matrix of input features, the nuclear repulsion forces $\mathbf{q}^{\mathrm{NR}}$ or a scaled version of them (see Supporting Information, Figure S1).

These inputs provide a complete representation, in that there is a one-to-one mapping between the $\mathbf{q}^{\mathrm{NR}}$ and the molecular geometry. The hidden blocks comprise a layer of 1000 neurons followed by a layer of N^q neurons (e.g. for aspirin, N^q is 210). The two-layer block design seeks to mitigate the vanishing gradient problem.[32] Retaining the dimensionality of the input and output forces is convenient for performing operations with them. Specifically, we draw inspiration from modern image classification networks, ResNets,[33] introducing shortcut connections which skip forward to blocks deeper in the network. By having these sorts of connections, each block is only required to learn a small transformation of the inputs and any residual information not captured in the output of a block is preserved for subsequent blocks.

As detailed above, we explore two different targets $\mathbf{q}^{\mathrm{NR}}$ as a reference for fitting, namely $\mathbf{q}^{\mathrm{QM}}$ (Equation 21, scheme **D1**) or $\mathbf{q}^{\mathrm{elec}}$ (Equation 22, scheme **D2**). As our networks use sigmoid activation functions in the final output layer, they can only yield values in the range 0 to 1. Consequently, we performed scaling of our reference training and predicted pairwise forces to this range. Details of these normalisation schemes for **D1** and **D2** are provided in Supporting Information (Figure S1). For all networks, the $\mathbf{q}^{\mathrm{NR}}$ input features were also normalised, as $\mathbf{q}^{\mathrm{NR}}/|\mathbf{q}^{\mathrm{NR}}_{\mathrm{max}}|$.

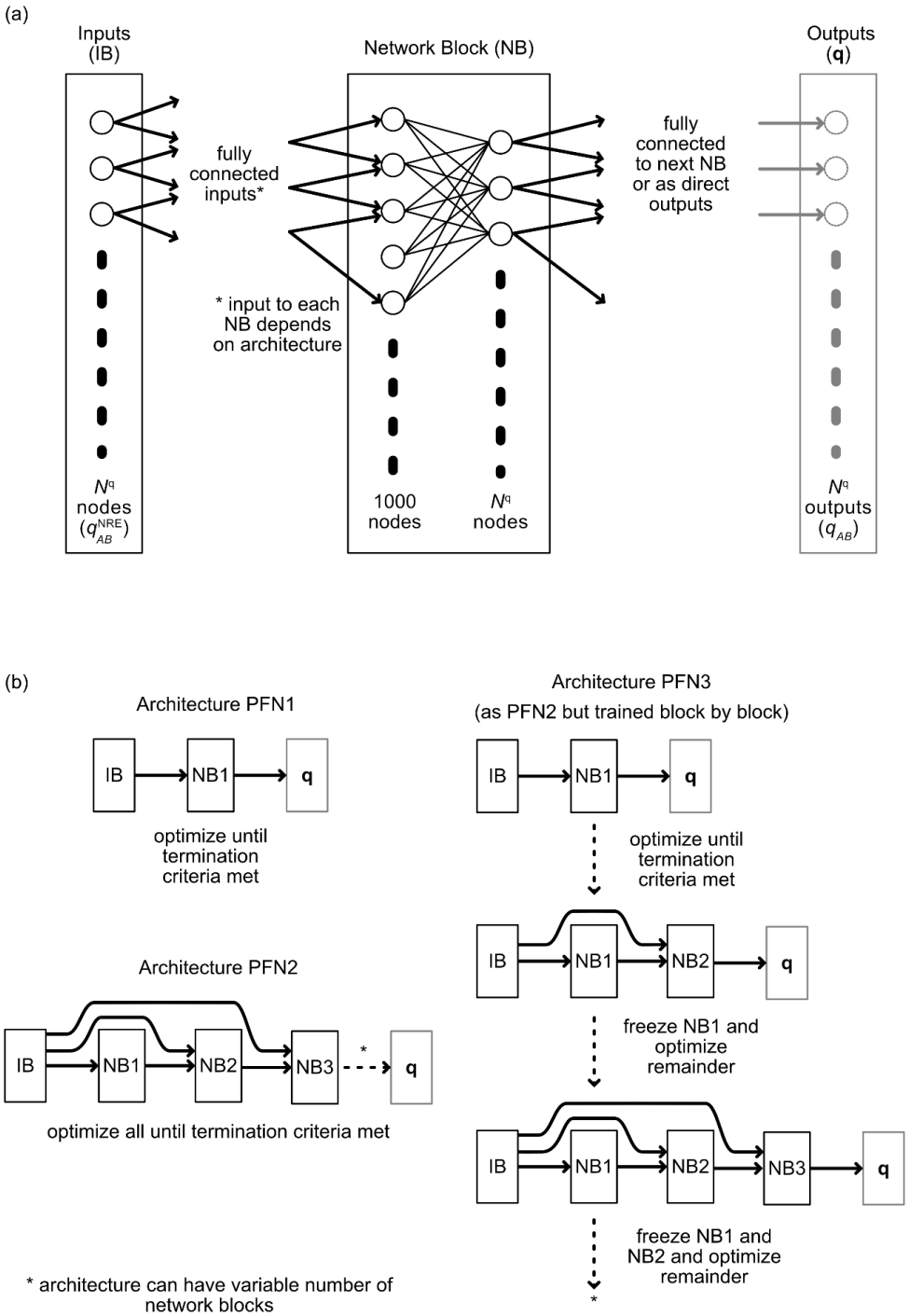

Figure 3 Artificial neural network architecture: (a) general structure of layers, network blocks (NB) and connectivity for input block (IB), NBs and output layer; (b) implemented network architectures **PFN1**, **PFN2** and **PFN3** and their training regimes. **PFN3** networks were evolved blockwise whereas **PFN1** and **PFN2** were fixed architectures. Direct and shortcut connections indicated by arrows.

3.2 Specific Network Architectures

Based on the general network template described above, we implemented a simple static network with a single hidden block (**PFN1**, Figure 3b). We also constructed static networks with more than one hidden block which employed shortcut connections (**PFN2**, Figure 3b). Finally, we evolved a network architecture in a stepwise fashion (**PFN3**, Figure 3b): this involved starting from a trained **PFN1** model, adding a further hidden network block with shortcut connections to the inputs; then retraining the network while freezing the weights of the preceding hidden block. This process, which we refer to as greedy blockwise training, was repeated until no further improvement in training performance was observed. Specifically, training was performed until no improvement was observed for 500 epochs or 100000 epochs had elapsed; this criterion proved suitable for ensuring convergence (for example, see Figure S2) and was applied to all three network types. The loss function that was minimised was the mean-square error in pairwise force, $\left\|\mathbf{q}^{\mathrm{Ref}} - \mathbf{q}^{\mathrm{ANN}}\right\|_2^2$. The networks were constructed using Keras (version 2.2.4)[31] with a TensorFlow backend (version 1.14.0). The Adam optimizer was used to minimise the loss function, applying the default parameters in Keras. In general, the networks were trained using a single NVIDIA V100 GPU and eight CPU cores and took approximately 3 - 10 s per epoch when training.

3.3. Atomic Force Datasets

To provide the reference atomic forces of different small organic molecule structures, needed for training and validating pairF-Net, we consider the MD17 database of Chmiela et al.[17] Specifically we consider three molecular entries in MD17 as suitably representative systems, namely aspirin, malonaldehyde and toluene (Figure 4). The geometries and forces in these datasets were generated as *ab initio* MD trajectories in the gas phase, with aspirin in its neutral form and malonaldehyde in its keto tautomer, conducted at a temperature of 500 K and timestep

of 0.5 fs, using the PBE + vdW-TS density functional. We derived our own training and test subsets from this database by sampling evenly across their potential energies, with the goal of obtaining a training set of size up to but no more than 50000. For aspirin, in order to maintain the even sampling criteria, a total of 42353 training structures were sampled with the remaining 169409 structures being added to the test set (Figure 4). No other criteria for selection of training data were used. The same process was carried out for the malonaldehyde and toluene sets (Figure 4).

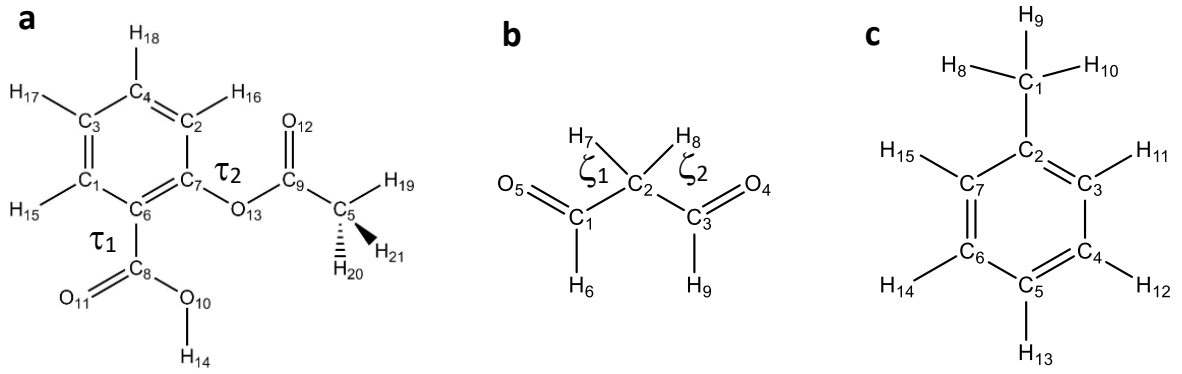

Figure 4 Structures, atom numbering and number of molecular structure-force datapoints for (a) aspirin, (b) malonaldehyde and (c) toluene. Number of molecule datapoints indicated in the format "(number in test set, number in training set)". Dihedral angles τ_1 and τ_2 in aspirin and ζ_1 and ζ_2 in malonaldehyde also indicated.

3.4 Network Performance

The performance of the trained pairF-Net models is evaluated by considering the resultant Cartesian atomic forces assembled from the predicted interatomic force components. Following Chmiela et al.[17], the error in magnitude of the Cartesian atomic forces is given as $||\mathbf{F}|| - ||\mathbf{F}^{QM}||$, where $\mathbf{F}$ is the predicted Cartesian force and $\mathbf{F}^{QM}$ is the reference Cartesian QM force; for this metric, both mean absolute error (MAE) and root-mean-square error (RMSE) values are computed. The corresponding MAE and RMSE errors in the angular components of

these forces are found by considering the measure, $\cos^{-1}(\frac{\mathbf{F}}{\|\mathbf{F}\|} \cdot \frac{\mathbf{F}^{\mathrm{QM}}}{\|\mathbf{F}^{\mathrm{QM}}\|})$. We also compute force error percentiles, presented as cumulative histograms of error plotted on a logarithmic scale; we refer to these below as S-curves.

4. Results and Discussion

4.1 Analysis of Pairwise Forces

To show our decomposition of total Cartesian force, $\mathbf{F}^{\mathrm{QM}}$, produces chemically reasonable pairwise forces, $\mathbf{q}^{\mathrm{QM}}$, we first apply it to a series of structures of aspirin. These structures and their corresponding total forces were obtained from three potential energy surfaces, obtained at the B3LYP/6-31G* level of density functional theory. The optimisations[34] were carried out for the aspirin conformer with minimum at $\tau_1 = 0.4°$ and $\tau_2 = 73.5°$, where τ_1 is defined as C_7-O_6-C_8-O_{11} and τ_2 as C_6-C_7-O_{13}-C_9 (Figure 4a).

The first two scans are along aspirin's $R(C_7\text{-}O_{13})$ and $R(C_8{=}O_{11})$ coordinates, corresponding to an ester C-O single bond and carboxylic acid carbonyl double bond respectively. The resulting decomposed force components **q** along these geometries are obtained via Equation 27 and indicate the expected potential energy curve for bonded atoms (Figure 5a): indeed, a suitably steeper curve is observed for the stiffer double bond of $C_8{=}O_{11}$. For both bonds, the decomposed force components **q** have the required properties of being smooth and continuous, and possessing a zero value at the potential energy stationary points, at distances of 1.38 Å and 1.22 Å for C_7-O_{13} and $C_8{=}O_{11}$ respectively (Figure 5a). Furthermore, they also have the expected property of being repulsive when the bonds are compressed and attractive as the bonds are extended.

The third potential energy scan is around dihedral angle τ_3 of aspirin, defined as C_1-C_6-O_8-C_{10} (Figure 5b). This corresponds to a 1–4 interaction between atoms $C_1 \cdots O_{10}$ within the phenyl and carboxylate groups respectively. Once again, the pairwise force components **q** vary continuously, in a characteristically sinusoidal fashion, and have a potential energy is zero at $\tau_3 = -1.0°$, corresponding to a 1–4 distance of 2.71 Å, between atoms C_1 and O_{10}.

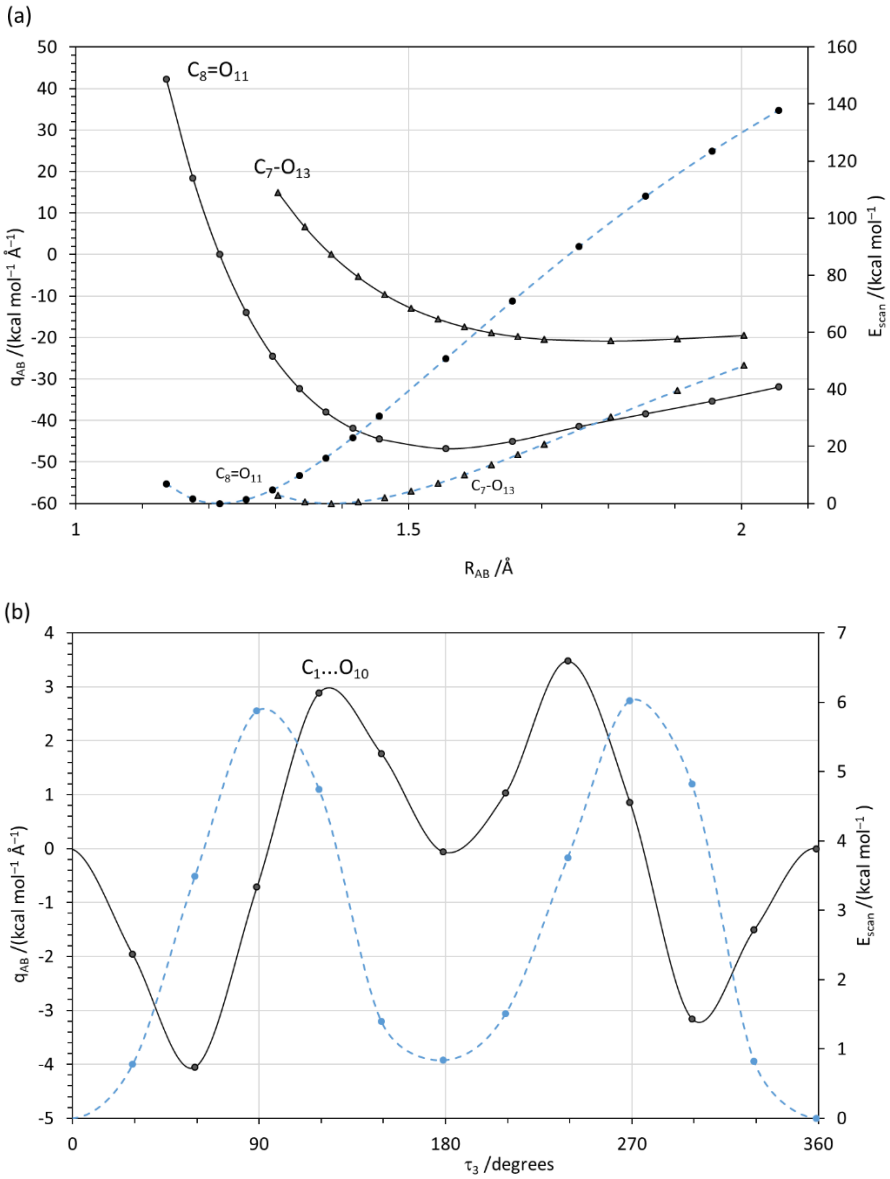

Figure 5 Interatomic force component q_{AB} (black solid lines) for aspirin (a) as a function of interatomic distance R_{AB} for bonds C_7-O_{13} and C_8=O_{11}; and (b) as a function of torsion angle τ_3: (b)

$C_1 \cdots O_{10}$ 1–4 interaction. The corresponding potential energy curves, E_{scan}, (blue dashed lines) are also shown for the three potential energy optimisation scans used to obtain the structures.

We also evaluate the suitability of nuclear repulsion force $\mathbf{q}^{\mathrm{NR}}$ as an input feature for prediction of $\mathbf{q}^{\mathrm{QM}}$ or its electronic component, $\mathbf{q}^{\mathrm{elec}}$. Firstly, we plot $\mathbf{q}^{\mathrm{elec}}$ against $\mathbf{q}^{\mathrm{NR}}$ for all interactions within the structures of the aspirin training dataset (Figure 6a). We note a strong inverse correlation between $\mathbf{q}^{\mathrm{NR}}$ and $\mathbf{q}^{\mathrm{elec}}$. Both quantities exhibit very large ranges, from zero to ~10^3 kcal mol^{-1} Å^{-1} in magnitude. The addition of these two large quantities of opposite sign (Equation 22) may portend problems in numerical accuracy regarding training and prediction. Next, we consider the corresponding plot of total pairwise force $\mathbf{q}^{\mathrm{QM}}$ against $\mathbf{q}^{\mathrm{NR}}$ (Figure 6b). Here, we note that the range of total force is considerably reduced, to ~10^2 kcal mol^{-1} Å^{-1}. In addition, various bands may be seen (Figure 6b). Similar banded clusters are observed for the malonaldehyde and toluene datasets (Supporting Information, Figure S3).

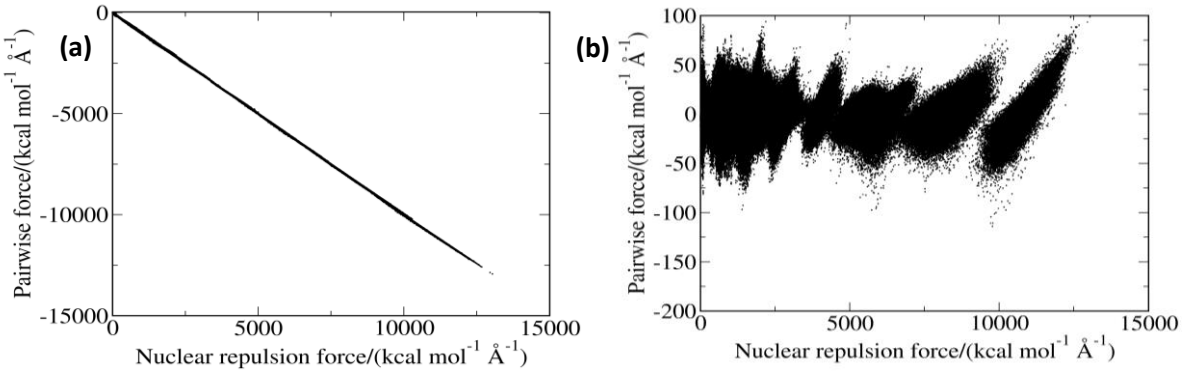

Figure 6 Plot of nuclear repulsion forces $\mathbf{q}^{\mathrm{NR}}$ against (a) $\mathbf{q}^{\mathrm{elec}}$ and (b) the total pairwise force $\mathbf{q}^{\mathrm{QM}}$, for the aspirin training set.

On further examination, these bands arise from the different types of interaction present in the molecules. For example, we focus on the separate bands arising from carbon-oxygen

interactions: those at higher values of nuclear repulsion force correspond to interactions between directly bonded atoms, as would be anticipated (Figure 7a,b); those clusters with lower internuclear repulsion involve more distant 1–3, 1–4 and higher interactions (Figure 7c,d,e). We observe that the nuclear repulsion force seems to correlate more strongly with the pairwise force $\mathbf{q}^{\mathrm{QM}}$ for 1–2 bonding interactions. Nevertheless, the $\mathbf{q}^{\mathrm{NR}}$ do indicate some ability to discriminate between physically distinct pairwise interactions, as is required for an effective input feature for network training.

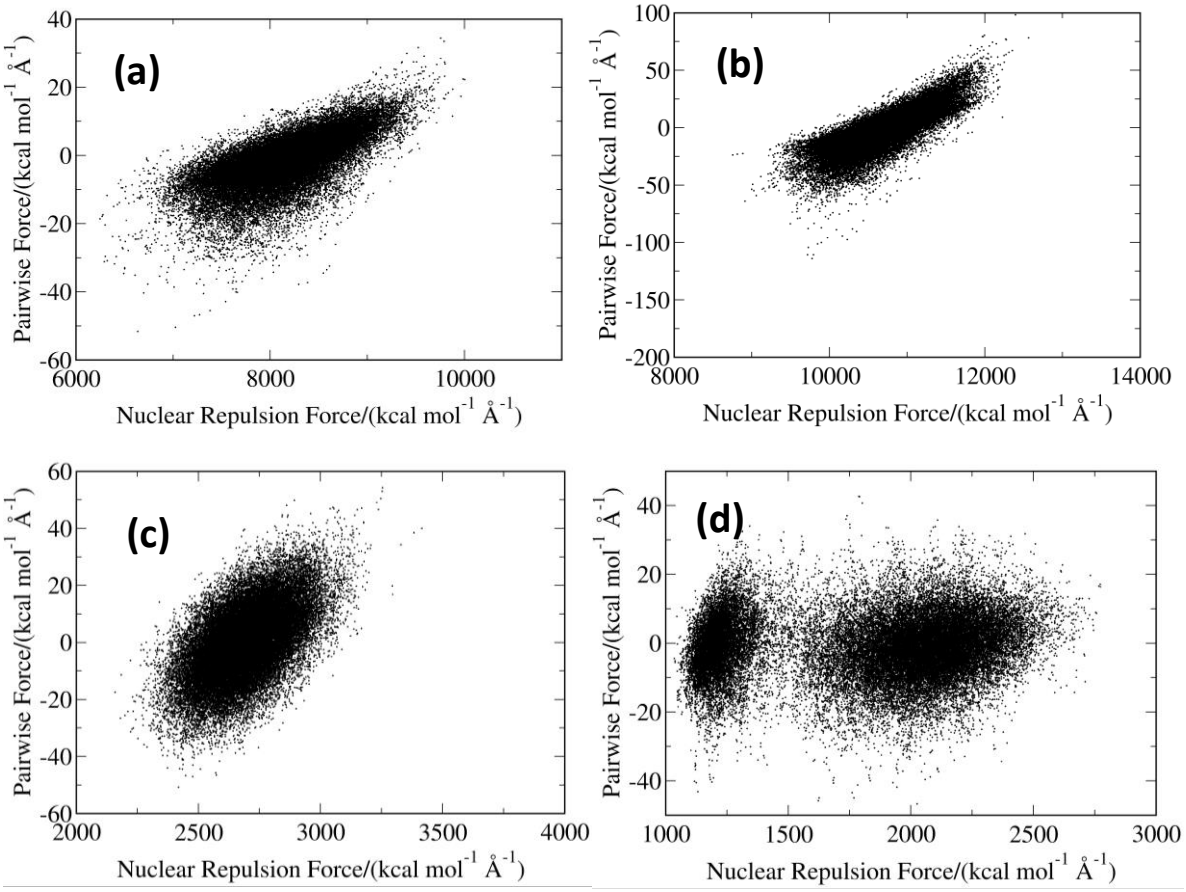

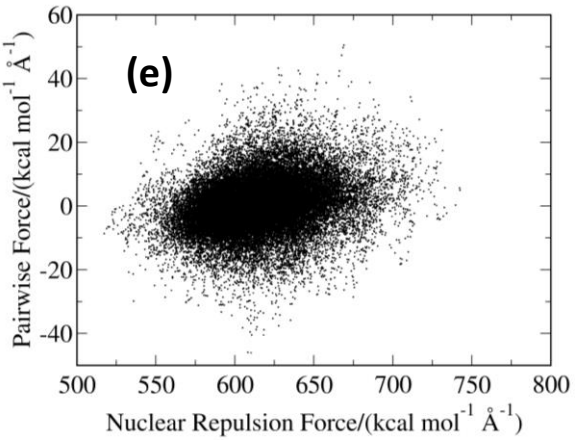

Figure 7 Plot of total pairwise force $\mathbf{q}^{\mathrm{QM}}$ against nuclear repulsion force $\mathbf{q}^{\mathrm{NR}}$ for different carbon-oxygen interactions in the aspirin training set, (a) singly bonded atoms C_7-O_{13} (b) doubly bonded atoms C_8=O_{11} (c) 1–3 interacting atoms $C_5\cdots O_{12}$ (d) 1–4 interacting atoms $C_1\cdots O_{10}$ and (e) 1–5 interacting atoms $C_4\cdots O_{11}$.

4.2 Network Optimisation

Therefore, the pairwise forces $\mathbf{q}^{\mathrm{Ref}}$ derived from the total Cartesian atomic forces **F** appear to exhibit suitable physical attributes of the molecular system. Next, we explore the ability of neural networks to predict **F** by learning the decomposed $\mathbf{q}^{\mathrm{Ref}}$ of the molecule. We focus here on aspirin (Figure 4a) as a challenging model system, with a variety of chemical functionality and conformational flexibility. A number of neural network architectures and training schemes are considered, as summarised in Table 1 (further details are given in Computational Details and Figure 3).

Table 1 Summary of network models trained and assessed in this work, including reference for fitting, **D1** ($\mathbf{q}^{\mathrm{QM}}$) and **D2** ($\mathbf{q}^{\mathrm{elec}}$); and architecture, i.e. presence of shortcut connections (residual); whether network was static or evolved (greedy blockwise); and number of blocks

(N_{block}). Input to all the networks were the derivatives of the internuclear repulsion energy as expressed in an interatomic basis, $\mathbf{q}^{NR}$.

model	reference	architecture	N_{block}
PFN3a	**D2**	greedy blockwise/residual	1
PFN2a	**D2**	static/residual	2
PFN1a	**D1**	static	1
PFN3b	**D1**	greedy blockwise/residual	5
PFN1b	**D1**	static	1
PFN2b	**D1**	static/residual	4
PFN2c	**D1**	static/residual	6

For training of the first pairF network, **PFN3a** (Table 1), we decompose the reference total forces $\mathbf{F}^{\mathbf{QM}}$ on atoms of aspirin for each of its ~50,000 structures into $\mathbf{q}^{elec}$ pairwise forces (scheme **D2**). We apply a greedy blockwise scheme to evolve the network architecture. According to the convergence criterion, only a single additional block was added to the network. The **PFN3a** was then applied to prediction of the forces within the test set of 1.7 x 10^5 aspirin structures, corresponding to 3.6 x10^6 force vectors. The resulting mean absolute error in total force was found to be 5.51 kcal mol^{-1} $Å^{-1}$ (Table 2). To explore the effect of network architecture manually, we also trained network **PFN2a** against $\mathbf{q}^{elec}$, consisting of a fixed two-block architecture without freezing any weights (Figure 3b, Table 1). However,

network **PFN2a** offered only a modest improvement on **PFN3a**, with an MAE of 4.83 kcal mol^{-1} $Å^{-1}$ (Table 2). Static network **PFN1a** was also constructed, comprised of a single hidden block, but crucially trained against total pairwise forces $\mathbf{q}^{QM}$ (scheme **D1**). The trained network yielded significantly improved performance, with a MAE in total force of 1.91 kcal mol^{-1} $Å^{-1}$ (Table 2).

Consequently, a second network with the **PFN3** architecture was developed in a greedy blockwise fashion. However, the target this time was total pairwise force **q** according to the **D1** scheme. This led to network **PFN3b**, with five hidden blocks (Table 1). This network exhibited further improvement on **PFN1a** and particularly over **PFN3a**, with a MAE in force of 1.72 kcal mol^{-1} $Å^{-1}$ (Table 2). For the former, the increased accuracy in prediction appears to stem mainly from improved prediction in the direction of the total force vector, with a lower angle MAE of 0.027 kcal mol^{-1} $Å^{-1}$ (Table 2).

Table 2: Accuracy of pairF network **PFN3b** for predicting Cartesian forces **F** of the aspirin, toluene and malonaldehyde test datasets. Errors in kcal $mol^{-1}Å^{-1}$.

pairF network	**Total**		**Magnitude**		**Angle**	
	MAE	**RMSE**	**MAE**	**RMSE**	**MAE**	**RMSE**
PFN3a	5.51	7.33	5.83	7.78	0.0898	0.1250
PFN2a	4.83	6.50	5.28	7.17	0.0758	0.1070
PFN1a	1.91	2.59	1.97	2.68	0.0303	0.0425
PFN3b	1.72	2.39	1.96	2.80	0.0268	0.0402
PFN1b	1.85	2.52	1.92	2.60	0.0296	0.0421

PFN2b	2.98	4.02	3.19	4.33	0.0463	0.0662
PFN2c	3.41	4.61	3.64	4.97	0.0530	0.0745

In order to examine if the greedy blockwise training method produces better results than simply using fixed blocks, networks **PFN2b** and **PFN2c** were constructed, with four and six hidden blocks respectively; both were trained according to scheme **D1** (Table 1). These networks exhibited a MAE in force of 2.98 and 3.41 kcal mol^{-1} $Å^{-1}$ respectively, with lower accuracy than **PFN3b** in both magnitude and direction of predicted force vectors (Table 2). This suggests that the greedy blockwise training is more effective than simultaneous training of an entire network. Additionally, network **PFN1b** was constructed, consisting of a single block that had 5000 rather than 1000 neurons in the first layer; the MAE in force was 1.85 kcal mol^{-1} $Å^{-1}$, slightly higher than found for **PFN3b** (Table 2).

Although it could be argued, based on MAE in force, that the performance of network **PFN3b** and e.g. **PFN1a** or **PFN1b** are very similar, it is important to consider not just the average force prediction error but also the distribution of errors. To this end, we also consider the percentage of pairwise force predictions made to an accuracy of 1 $kcal^{-1}$ mol^{-1} $Å^{-1}$, which we denote as metric, L1. We find the $L1_{test}$ value for **PFN3b** is 68.8% (Table 3), indicating that 68.8% of the 3.6×10^6 force vectors in the aspirin test set were predicted to an accuracy of 1 $kcal^{-1}$ mol^{-1} $Å^{-1}$ or better. By contrast, the $L1_{test}$ values for **PFN1** and **PFN1b** were 48.0% and 49.0% respectively (Table 2). Furthermore, network **PFN3a** achieved an $L1_{test}$ of only 25.6%.

Table 3 Fraction of points with MAE in pairwise forces $\mathbf{q}^{QM}$ or $\mathbf{q}^{elec}$ of less than kcal mol^{-1} Å^{-1} for prediction of aspirin test set ($L1_{test}$) and training set, $L1_{train}$ (in parentheses) by neural network models.

pairF network	**$L1_{test}$ ($L1_{train}$)**
PFN3a	25.8 (26.0)
PFN2a	31.0 (32.0)
PFN1a	48.0 (49.5)
PFN3b	68.8 (76.7)
PFN1b	49.0 (51.2)
PFN2b	45.2 (46.3)
PFN2c	37.6 (38.2)

4.3 Application of PairF Network PFN3b

Given the ability of pairF-Net **PFN3b** to provide the most accurate forces for aspirin, we next apply this network to two other small organic molecules, malonaldehyde and toluene (Figure 4). As before, a network was trained for each molecule according to scheme **D1**, based on pairwise decomposition of the atomic force datasets of the MD17 database (Figure 4). The MAEs in total force for the trained **PFN3b** networks when applied to the malonaldehyde and toluene test sets were 0.54 and 1.25 kcal^{-1} mol^{-1} Å^{-1} respectively (Table 4). The very good performance of **PFN3b** for the malonaldehyde test set, which contains ten times more molecular structures than in its training set (Figure 4), does appear to arise in particular from a low angle MAE of 0.0099 kcal^{-1} mol^{-1} Å^{-1} (Table 4), i.e. it predicts well the sign of the force components as well as the magnitude. We also consider the spread of errors according to L1 values: again, malonaldehyde has the best performance, with a $L1_{test}$ value of 87.9% compared to 58.4% for toluene and 68.8% for aspirin (Table 4).

Table 4 Accuracy of pairF network **PFN3b** for predicting Cartesian forces **F** of the aspirin, toluene and malonaldehyde test datasets (L1 for training datasets given in parentheses). Errors in kcal mol^{-1} $Å^{-1}$.

Molecule	**Total**		**Magnitude**		**Angle**		**$L1_{test}$**
	MAE	**RMSE**	**MAE**	**RMSE**	**MAE**	**RMSE**	**($L1_{train}$)**
aspirin	1.72	2.39	1.96	2.80	0.0268	0.0402	68.8 (76.7)
malonaldehyde	0.54	0.72	0.58	0.77	0.0099	0.0147	87.9 (90.8)
toluene	1.25	1.71	1.44	1.97	0.0200	0.0300	58.4 (65.8)

We may also consider the spread of errors according to their force error percentiles; these cumulative distributions take an S-shaped form and we refer to them subsequently as S-curves. We observe broadly similar S-curve profiles for aspirin, malonaldehyde and toluene (Figure 8). The value of these curves at an error of 1 $kcal^{-1}$ mol^{-1} $Å^{-1}$ corresponds to the L1 values reported in Tables 3 and 4. Specifically, the good performance in prediction of forces for malonaldehyde is reflected in a larger intercept value on the x-axis, of 18 $kcal^{-1}$ mol^{-1} $Å^{-1}$, as compared to values of 10 and 9 $kcal^{-1}$ mol^{-1} $Å^{-1}$ for aspirin and toluene, respectively (Figure 8). Furthermore, the S-curve plateaus at a lower error for malonaldehyde than the other two molecules, at a value of 3 $kcal^{-1}$ mol^{-1} $Å^{-1}$ (Figure 8b), indicating a narrower range of errors for this molecule.

An interesting comparison of these network predictions of total force is with that furnished by a quantum chemical model. Therefore, we compute forces on the aspirin atoms of aspirin in the training set via the semiempirical QM Hamiltonian, PM6.[35] The S-curve for PM6 (the red curve in Figure 8a) appears significantly right-shifted relative to the **PFN3b** profile, with errors

occurring in excess of 10 kcal^{-1} mol^{-1} Å^{-1}. The PM6 predictions have an associated $L1_{train}$ value of only 38.1%, indicating notably poorer performance than the **PFN3b** network in reproducing the PBE + vdW-TS forces.

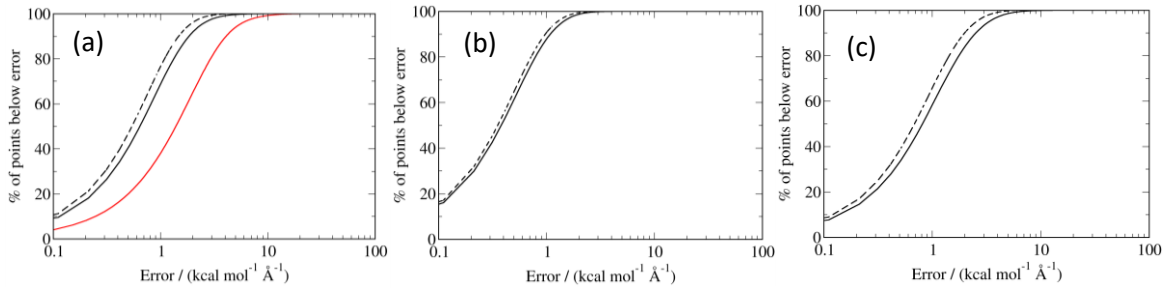

Figure 8 Force error percentile S-curves for (a) aspirin, (b) malonaldehyde and (c) toluene, using neural network **PFN3b** applied to the training data set of forces (dotted black), the test data set of forces (solid) and, for aspirin, *via* the PM6 Hamiltonian (red) for the forces acting on the atoms in the training data set. The error is defined as $\left\|\mathbf{q}^{\mathrm{Ref}} - \mathbf{q}^{\mathrm{ANN}}\right\|_2$.

To assess how well the network **PFN3b** predicts interactions between different atom types, we consider the distribution of accuracy measure L1 across atom pairs (Figure 9). For aspirin, it is evident that the interactions fall into two approximately equally sized sets (Figure 9a), one with a set of L1 values of 70% or more, and a second set of less well predicted pairwise forces, with L1 values of 60% or less. This profile also appears to be reflected in other networks, eg. static **PFN2b** (Figure 9b). Within the latter set is a group of interactions indexed as #148 to #210 (Figure 9a). These involve aromatic hydrogens H_{16}, H_{17} and H_{18} of the phenyl group and the methyl group hydrogens; it would appear to suggest some complexity in their coupling to other regions of the aspirin molecule. Also less well predicted in aspirin are the forces for interactions #36 to #65 (Figure 9a) involving carboxylic acid oxygen atoms O_{10} and O_{11}. Similarly lower predictive accuracy is found for the methyl hydrogens within toluene (#25 to #42, Figure 9d); this again may indicate some subtlety in their interatomic interactions.

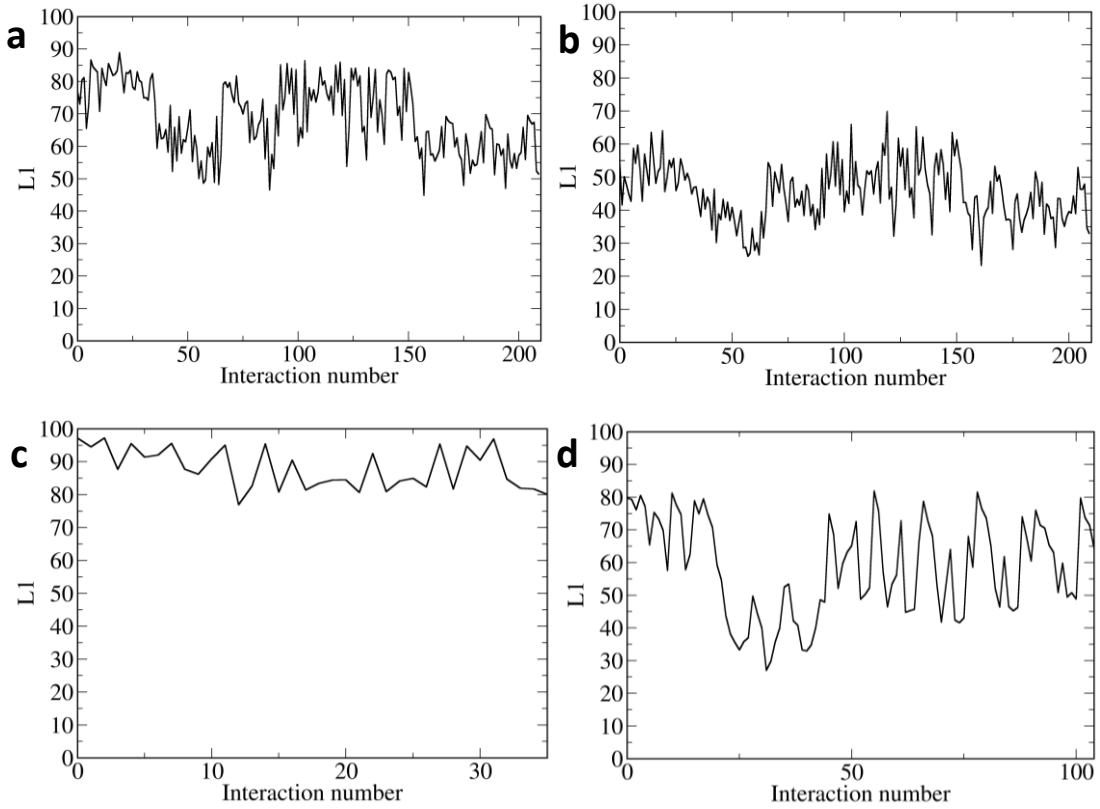

Figure 9 The percentage of points with an error below 1 $kcal^{-1}$ mol^{-1} $Å^{-1}$ (L1) for each pairwise force prediction for networks (a) **PFN3b** and (b) **PFN2b** for the aspirin test set; and **PFN3b** for (c) malonaldehyde and (d) toluene test sets.

However, as expected from preceding analyses above, the L1 values for interactions within malonaldehyde do not fall below 70%, indicating a good ability to reproduce the pairwise forces for test set geometries of this small molecule (Figure 9c). These test structures are *ab initio* MD simulation geometries of malonaldehyde, obtained from the reference MD17 database (see Methods). Indeed, when we use the **PFN3b** network here for force prediction, to guide a molecular dynamics simulation of malonaldehyde *in vacuo*, we observe the generation of conformations lying within the manifold of the MD17 phase space (Figure 10): the **PFN3b** trajectory samples well in the broad low energy region around OCCC torsion angles (ζ_1,ζ_2) of

(100°,100°) and begins to sample the symmetric (-100°,-100°) region (red, Figure 10). Both of these regions are well populated in the MD17 data set (black, Figure 10).

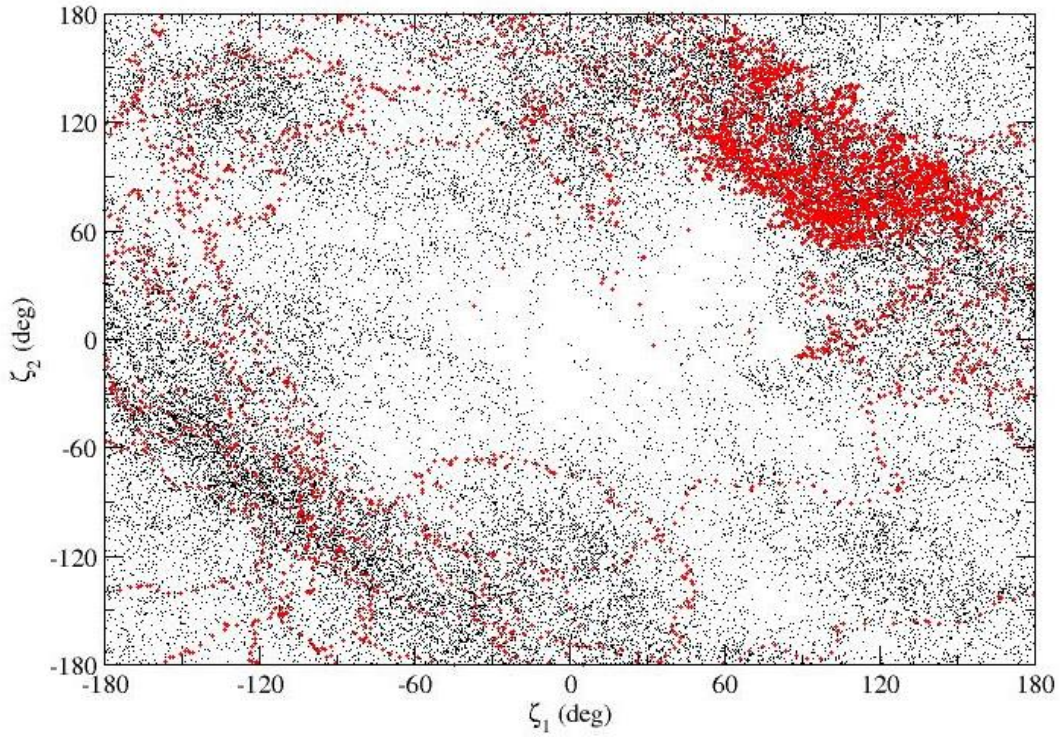

Figure 10 Molecular dynamics trajectory of OCCC torsion angles ζ_1 and ζ_2 (in deg) of malonaldehyde in the gas phase over 20 ps, using forces generated by the **PFN3b** network (red); and comparison with sampled points from MD17 database (black). Angles ζ_1 and ζ_2 defined in Figure 4. Simulation performed in microcanonical ensemble with timestep of 0.5 fs and initial velocities calculated from the forces.

5. Conclusions

In this work, we have introduced the pairF-Net approach to predict atomic forces. For the small organic molecules considered here, the best pairF-Net model yields an MAE in total atomic Cartesian force prediction on the order of 1 $kcal^{-1}$ mol^{-1} $Å^{-1}$. This error in prediction is comparable to other machine learned force predictions methods such as GDML[17] and DPMD.[19] The strength of the pairF-Net method is in its chemically intuitive simplicity, with the application of an artificial neural network to learn the pairwise forces between atoms, needing to make only scalar predictions to predict vector quantities in an intuitive manner. The pairwise

forces obtained from decomposition of the total atomic forces are straightforward to obtain from decomposition of the total atomic forces and capture expected features of interatomic interactions, such as bond curves and periodic torsional potentials. In adopting this approach to constructing a force potential from pairwise forces, the method resembles a molecular mechanical force field approach but without making *a priori* assumptions about the functional form of atomic interactions.

Our best performing network for prediction of force, **PFN3b**, is obtained *via* dynamic evolution of its architecture. We also find fitting of total pairwise force $\mathbf{q}^{\mathrm{QM}}$ is superior to fitting only the electronic term $\mathbf{q}^{\mathrm{elec}}$. In part, the lower performance in fitting to $\mathbf{q}^{\mathrm{elec}}$ reflects the greater numerical challenge of fitting these very large magnitude quantities and then adding them to sizable $\mathbf{q}^{\mathrm{NR}}$ values to produce a smaller total $\mathbf{q}^{\mathrm{Ref}}$ and from that, the reconstructed total **F**. Furthermore, we note that $\mathbf{q}^{\mathrm{elec}}$ is obtained as the solution to coordinate transformation with minimum Euclidian norm; while the pairwise force **q** adopts the expected profile (eg. Figure 5), there is no guarantee that $\mathbf{q}^{\mathrm{elec}}$ will exactly equate to the physically correct electronic pairwise forces in the molecular system.

Although the performance of the pairF-Net approach is encouraging, we note that some interactions, particularly within toluene and aspirin, are less well predicted. These are larger molecules than malonaldehyde and have rather more interactions to be learned. Consequently, further refinement of the scheme is underway to develop alternative decomposition schemes and input parameters, as well as to incorporate permutational invariance, which would aid in the accurate modelling of carboxylate oxygens and methyl hydrogens for example. A further point to note with respect to applying these force models within molecular dynamics simulations is the need for judicious selection of training data points. The training sets for these

molecules, having been derived from AIMD simulations, and although acquired at 500 K, still largely sample around low energy structures (Figures 10 and S4). Thus, regions of transition between conformers are therefore less well represented and may lead to problems in force prediction when these intermediate structures are encountered during MD simulations. Consequently, more complete training sets may be required, eg. from adaptive sampling schemes[15] or other methods to generate suitable datapoints.

Supporting Information

Information on normalisation scheme, network convergence and further analyses of pairwise forces and training data set.

Acknowledgements

We thank the EPSRC for funding (EP/R512035/1) and use of the JADE high performance computing facility. We also thank Dr Andrew Grant (Atos) and the STFC Hartree Centre for their contributions. The authors would also like to acknowledge the use of the Computational Shared Facility at the University of Manchester.

References

1. Salomon-Ferrer, R.; Götz, A. W.; Poole, D.; Le Grand, S.; Walker, R. C., *J. Chem. Theory Comput.* **2013**, *9*, 3878-3888.
2. Dror, R. O.; Dirks, R. M.; Grossman, J.; Xu, H.; Shaw, D. E., *Annu. Rev. Biophys.* **2012**, *41*, 429-452.
3. Buch, I.; Giorgino, T.; De Fabritiis, G., *Proc. Natl. Acad. Sci. USA* **2011**, *108*, 10184-10189.

4. Alibay, I.; Burusco, K. K.; Bruce, N. J.; Bryce, R. A., *J. Phys. Chem. B* **2018**, *122*, 2462-2474.

5. Alibay, I.; Bryce, R. A., *J. Chem. Inf. Model.* **2019**, *59*, 4729-4741.

6. Lindorff-Larsen, K.; Piana, S.; Dror, R. O.; Shaw, D. E., *Science* **2011**, *334*, 517-520.

7. Fink, T.; Reymond, J.-L., *J. Chem. Inf. Model.* **2007**, *47*, 342-353.

8. Merz Jr, K. M., *Acc. Chem. Res.* **2014**, *47*, 2804-2811.

9. Behler, J., *J. Chem. Phys.* **2016**, *145*, 170901.

10. Smith, J. S.; Isayev, O.; Roitberg, A. E., *Chem. Sci.* **2017**, *8*, 3192-3203.

11. Gastegger, M.; Marquetand, P., *J. Chem. Theory Comput.* **2015**, *11*, 2187-2198.

12. Dral, P. O.; Owens, A.; Yurchenko, S. N.; Thiel, W., *J. Chem. Phys.* **2017**, *146*, 244108.

13. Shen, L.; Wu, J.; Yang, W., *J. Chem. Theory Comput.* **2016**, *12*, 4934-4946.

14. Gastegger, M.; Behler, J.; Marquetand, P., *Chem. Sci.* **2017**, *8*, 6924-6935.

15. Smith, J. S.; Nebgen, B.; Lubbers, N.; Isayev, O.; Roitberg, A. E., *J. Chem. Phys.* **2018**, *148*, 241733.

16. Botu, V.; Ramprasad, R., *Phys. Rev. B* **2015**, *92*, 094306.

17. Chmiela, S.; Tkatchenko, A.; Sauceda, H. E.; Poltavsky, I.; Schütt, K. T.; Müller, K.-R., *Sci. Adv.* **2017**, *3*, e1603015.

18. Schütt, K. T.; Sauceda, H. E.; Kindermans, P.-J.; Tkatchenko, A.; Müller, K.-R., *J. Chem. Phys.* **2018**, *148*, 241722.

19. Zhang, L.; Han, J.; Wang, H.; Car, R.; Weinan, E., *Phys. Rev. Lett.* **2018**, *120*, 143001.

20. Rupp, M.; Tkatchenko, A.; Müller, K.-R.; Von Lilienfeld, O. A., *Phys. Rev. Lett.* **2012**, *108*, 058301.

21. Ramakrishnan, R.; Dral, P. O.; Rupp, M.; Von Lilienfeld, O. A., *Sci. Data* **2014**, *1*, 140022.

22. Smith, J. S.; Isayev, O.; Roitberg, A. E., *Sci. Data* **2017**, *4*, 170193.

23. Behler, J., *J. Chem. Phys.* **2011**, *134*, 074106.

24. Adamo, C.; Barone, V., *J. Chem. Phys.* **1999**, *110*, 6158-6170.

25. Tkatchenko, A.; Scheffler, M., *Phys. Rev. Lett.* **2009**, *102*, 073005.

26. Wilson, E. B.; Decius, J. C.; Cross, P. C., *Molecular Vibrations: The Theory of Infrared and Raman Vibrational Spectra*; New York: McGraw-Hill, 1955.

27. Peng, C.; Ayala, P. Y.; Schlegel, H. B.; Frisch, M. J., *J. Comput. Chem.* **1996**, *17*, 49-56.

28. Stauch, T.; Dreuw, A., *Chem. Rev.* **2016**, *116*, 14137-14180.

29. Avdoshenko, S. M.; Konda, S. S. M.; Makarov, D. E., *J. Chem. Phys.* **2014**, *141*, 134115.

30. Abadi, M.; Agarwal, A.; Barham, P.; Brevdo, E.; Chen, Z.; Citro, C.; Corrado, G. S.; Davis, A.; Dean, J.; Devin, M., **2016**, arXiv:1603.04467.

31. Chollet, F., *Astrophysics Source Code Library* **2018**, ascl: 1806.022.

32. Hochreiter, S.; Bengio, Y.; Frasconi, P.; Schmidhuber, J., Gradient Flow in Recurrent Nets: The Difficulty of Learning Long-Term Dependencies. A field guide to dynamical recurrent neural networks. IEEE Press: 2001.

33. He, K.; Zhang, X.; Ren, S.; Sun, J. In *Deep Residual Learning for Image Recognition*, Proceedings of the IEEE conference on computer vision and pattern recognition, 2016; pp 770-778.

34. Frisch, M. J., et al. *Gaussian 16 Rev. A.03*, Wallingford, CT, 2016.

35. Stewart, J. J., *J. Mol. Model.* **2007**, *13*, 1173-1213.